Development of Block Cores Comprising High-B_S Nanocrystalline Alloy Ribbon

Motoki Ohta[1], Ryusuke Hasegawa[2], and Hiromitsu Itabashi[1]

[1]Hitachi Metals Ltd., Yasugi 692-8601, Japan
[2]Metglas Inc., Conway, SC 29526 USA

Soft magnetic properties of block cores comprising $Fe_{bal.}Cu_1Mo_{0.2}Si_4B_{14}$ nanocrystalline alloy ribbons (HBN core) were investigated. The HBN core shows a magnetic flux density at 2000 A/m (B_{2000}) of 1.73 T, which is about 0.2 T higher than that of the core comprising Fe-based amorphous alloy ribbons (Fe-AM core). The core loss at 200 mT and 10 kHz is 8.5 W/kg, two thirds of that of the Fe-AM core. The coefficient of the excess eddy current loss for the HBN core is one half of that of the Fe-AM core; the difference in core loss is prominent at higher frequencies.

Index Terms—**Block core, high- B_S soft magnetic materials, nanocrystalline magnetic materials.**

I. Introduction

HIGH power density is essential for the miniaturization of power inductive components such as transformers and/or reactors. To realize high power output from a component, operating frequency (switching frequency) is being increased year after year [1]–[3]. Components operating in medium frequency ranges (1–50 kHz) are coming under spotlight owing to the development of high-performance semiconductor power devices using SiC and GaN [4], [5]. In these frequency ranges, the operating magnetic flux density, B_m, of a given component is determined by heat due to the core loss; therefore, minimal core loss is desirable. On the other hand, high-saturation magnetic flux density, B_s, is required for larger superimposed current, especially for reactors. Materials with desired characteristics in medium frequency application fields include 6.5 wt.% Si-Fe alloy, Fe-based amorphous alloys, and Fe-based nanocrystalline alloys. The 6.5 wt.% Si-Fe alloy exhibits a high B_s of 1.8 T, with near-zero magnetostriction [6], [7]. However, the core loss of a core assembled with this alloy at 10 kHz is three times larger than that of the Fe-based amorphous alloy ribbons [6]–[8], and hence, these materials are not likely to be competitive in the same application field. A core comprising a conventional Fe-based nanocrystalline alloy, such as Fe-Nb-Cu-Si-B, exhibits a remarkably low core loss of <2 W/kg at 0.2 T and 10 kHz but the B_s values of these alloys are <1.5 T [7]. A core comprising the Fe-based amorphous alloy ribbon (hereafter Fe-AM core) has one of the most optimized characteristics with high B_s and low core loss for medium frequency reactors [7]. The purpose of this paper is to develop a core with higher B_s and lower core loss than the Fe-AM core. In our previous study, we developed nanocrystalline Fe-Cu-B and Fe-Cu-Si-B alloys exhibiting B_s of higher than 1.8 T and coercivity, H_c, of lower than 7 A/m [8], [9]. In the as-quenched state of this material, primary crystals of number density of 1000 particles/μm^2 exist [8], [9]. By annealing this material in the temperature range of 400 °C∼500 °C, the nanocrystalline grains of average size of 20 nm grow [8], [9]. Since it requires certain amount of primary crystals in the as-quenched state, we had an issue of quenching-rate control during the casting. Therefore, we modified the Cu content to less than 1 at.%, in order to avoid creation of primary crystals in the as-quenched state [10]. Cu played a role of creation of primary crystals; however, its influence becomes small when the content is reduced. For these new modified materials, it was found that the average crystalline grain size becomes a function of the heating rate in the annealing process [10]. For example, the average grain size of $Fe_{82}Cu_1Nb_1Si_4B_{12}$ alloy is about 50 nm in the specimen with heating rate of 0.3 °C/s, whereas it is about 15 nm in that of 3 °C/s, and those H_c are 150 and 3.2 A/m, respectively [10]. Moreover, it was found that average grain size varied with the Nb content. Namely, higher the Nb content, smaller the grain size [11]. We assume that Nb or such elements that play a role of stabilizing amorphous phase could be reduced when the heating rate becomes high. In a recent study, we have developed an annealing equipment in which heating rate is over 100 °C/s, and toroidal cores were assembled with $Fe_{bal.}Cu_1Mo_{0.2}Si_4B_{14}$ nanocrystalline alloy [12]. The core exhibits a magnetic flux density, B_{800}, of 1.73 T at 800 A/m and the core loss of <8 W/kg at 0.2 T and 10 kHz [12]. Therefore, a core comprising this material could be an improvement over the Fe-AM cores. However, handling capability, effect of impregnation resin, and size variation remain important issues in the field. Thus, we focused on the assembling of the block cores. It is necessary to apply a high heating rate (>100 °C/s) during annealing to obtain a uniform nanocrystalline phase. Since the saturation magnetostriction, λ_s, of this material is 15×10^{-6}, residual stress would cause lower permeability and degrade the soft magnetic properties. Therefore, it is necessary to carry out annealing at a high heating rate without deforming thin metallic ribbons.

II. Experiment

In this paper, the chemical composition of the alloy ribbon is $Fe_{bal.}Cu_1Mo_{0.2}Si_4B_{14}$. An alloy ingot was melted by induc-

Manuscript received October 24, 2017; revised December 7, 2017; accepted January 9, 2018. Date of publication February 13, 2018; date of current version April 17, 2018. Corresponding author: M. Ohta (e-mail: motoki.ota.tw@hitachi-metals.com).

Color versions of one or more of the figures in this paper are available online at http://ieeexplore.ieee.org.

Digital Object Identifier 10.1109/TMAG.2018.2794378

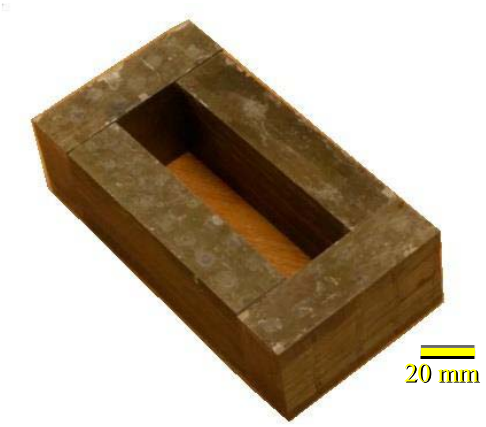

Fig. 1. Block core comprising $Fe_{bal.}Cu_1Mo_{0.2}Si_4B_{14}$ nanocrystalline alloy ribbon (HBN core).

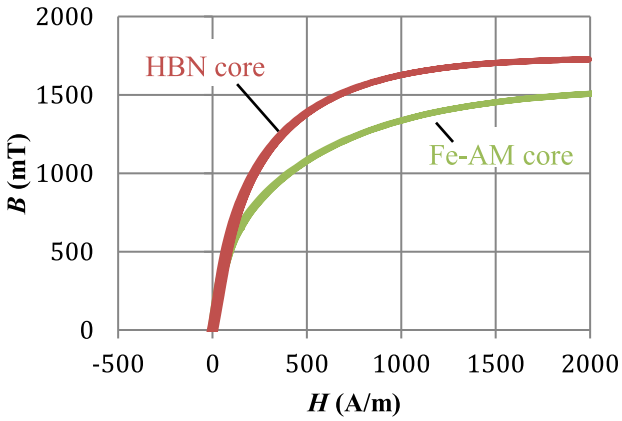

Fig. 2. B–H curves of block core comprising $Fe_{bal.}Cu_1Mo_{0.2}Si_4B_{14}$ nanocrystalline alloy ribbon (HBN core) and Fe-based amorphous alloy ribbon core (Fe-AM core).

tion heating in an Ar gas atmosphere. The ingot weighting about 20 kg was cast into 25.4 mm-wide amorphous ribbon with thickness of 23–25 μm by the melt-quenching method. The crystallization temperatures T_{X1} and T_{X2} measured by differential scanning caloricmeter were approximately 480 °C and 530 °C, respectively. Here, T_{X1} and T_{X2} denote the precipitation temperature of bcc Fe and Fe-B compounds, respectively. Note that, we find that it is possible to obtain fine nanocrystalline grain phases with Mo-free $Fe_{bal.}Cu_1Si_4B_{14}$ concentration. However, because of the decrease of the temperature difference between T_{X2} and T_{X1}, desired annealing temperature range becomes too narrow to control and the magnetic properties of single strips becomes too sensitive against soaking temperature in $Fe_{bal.}Cu_1Si_4B_{14}$ alloy. Therefore, in this paper, we employed $Fe_{bal.}Cu_1Mo_{0.2}Si_4B_{14}$ alloy. To anneal ribbons with a radius of curvature larger than 500 mm, we developed a roll-to-roll continuous in-line system and carried out annealing at 500 ± 2 °C for 2 s. According to TEM observation, the average grain size of the annealed ribbon was about 15 nm.

The annealed ribbons were cut to approximately the size of the blocks, and then, they were stacked and molded. The binder used for molding was an epoxy resin. Blocks were cut to the intended size and their side surfaces were chemically etched after grinding. Fig. 1 shows the block core comprising the $Fe_{bal.}Cu_1Mo_{0.2}Si_4B_{14}$ nanocrystalline alloy ribbon (HBN core). The corners were attached to each other to make a quasi-closed magnetic circuit with dimensions L: $121 \times W : 63 \times t : 35$ mm. DC B–H curve measurements were carried out by a B–H tracer using the primary and secondary turns of 60 and 6, respectively. AC-magnetic measurements were carried out using six primary and four secondary turns. Metglas AMCC-32 cores comprising an Fe-based amorphous alloy ribbon were also tested for comparison. The outer dimensions of the AMCC-32 core are $L : 82 \times W : 41 \times t : 30$. Magnetic domain observations were carried out using a wide-view magnetic domain observation microscope.

III. Result and Discussion

Fig. 2 shows the dc B–H curve of the HBN core and the Fe-AM core. Values of the magnetic flux density at 2000 A/m, B_{2000}, residual magnetic flux density, B_r, coercivity, H_c, and core loss at 0.2 T at 10 kHz, $P_{2/10k}$, and at 0.1 T at 20 kHz, $P_{1/20k}$, of these cores are shown in Table I. The value of B_{2000} of the HBN core is 1.73 T (=1730 mT) and that of the Fe-AM core is 1.50 T (1500 mT). We accordingly envision a notable advantage of the dc superimposing characteristics in the reactor of the HBN core. Furthermore studies on the reactor are underway. Note that B_{2000} of the HBN core is ~99% of B_s, whereas it is ~96% for the Fe-AM core. The difference in B_{2000}, i.e., the saturation behavior of the magnetic flux density, results from stress sensitivity. Fig. 3 shows the operating frequency f dependence of core loss P, with the operating flux density B_m of 0.2 T of the HBN core and the Fe-AM core. At 10 kHz, the HBN core shows a core loss of 8.5 W/kg, whereas the Fe-AM core shows 12.7 W/kg. The hysteresis loss, classical eddy current, and excess eddy current loss contribute to the total core loss [10], [11]. The relationship between P and f is given by

$$P = af + cf^2 + bf^{1.5} \tag{1}$$

where a, b, and c stand for the coefficient of the hysteresis loss, excess eddy current loss, and classical eddy current loss, respectively. A conventional method to separate the hysteresis loss and the classical eddy current loss is to divide both sides

TABLE I
Magnetic Flux Density at 2000 A/m, B_{2000}, Residual Magnetic Flux Density, B_r, Coercivity, H_c, and Core Loss at 0.2 T at 10 kHz, $P_{2/10k}$, and at 0.1 T at 20 kHz, $P_{1/20k}$ of Block Cores Comprising HBN Core and Fe-AM Core

	HBN core	Fe-AM core
B_{2000} (T)	1.73	1.50
B_r (T)	0.10	0.09
H_c (A/m)	14.2	10.6
$P_{2/10k}$ (W/kg)	8.5	12.7
$P_{1/20k}$ (W/kg)	5.4	7.7

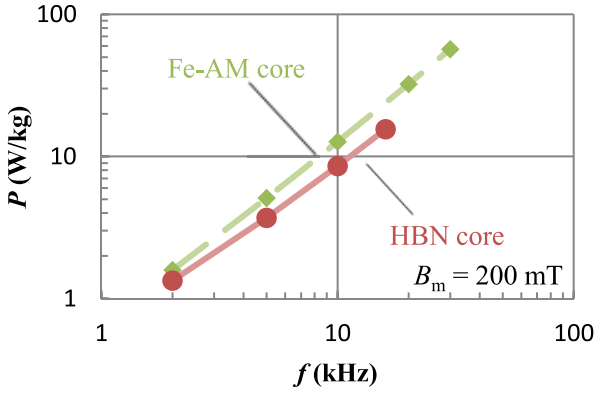

Fig. 3. Operating frequency f dependence of core loss P with operating flux density B_m of 200 mT for block core comprising $Fe_{bal.}Cu_1Mo_{0.2}Si_4B_{14}$ nanocrystalline alloy ribbon (HBN core) and Fe-based amorphous alloy ribbon core (Fe-AM core).

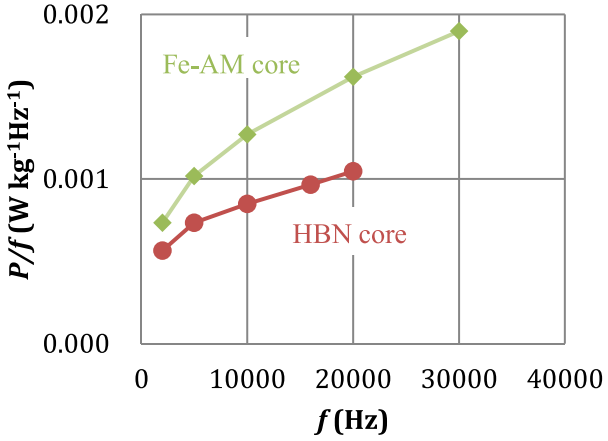

Fig. 4. P/f versus f plot of block core comprising $Fe_{bal.}Cu_1Mo_{0.2}Si_4B_{14}$ nanocrystalline alloy ribbon (HBN core) and Fe-based amorphous alloy ribbon core (Fe-AM core).

of (1) by f

$$P/f = a + cf + bf^{0.5}. \tag{2}$$

If the main contribution to the total loss stems from the classical eddy current in these frequencies, the relationship between P/f and f should be linear. However, as shown in Fig. 4, these parameters do not show a linear relationship. Namely, the coefficient c in (2) is small. According to Willard *et al.* [15], it is pointed out that classical eddy current losses for the ribbon alloys are negligibly small because of the skin effects at high frequencies. Note that, the thick oxide layer was confirmed on the surface of the present alloy prepared by the present annealing method in our previous study. In addition, impregnation resin prevents electrical contact between the layers. This suggests that each layer is electrically separated, suppressing classical eddy current in this core. Fig. 5 shows the P/f versus $f^{0.5}$ plot, where we can distinguish the proportional contribution of the excess eddy current, which is dominant at these frequencies. The coefficient of the excess eddy current b is expressed by

$$b = 8\left(G^{(w)}Sh_0/\rho_e\right)^{0.5} \cdot B_m^{1.5} \tag{3}$$

where $G^{(w)}$ is a geometric factor, $G^{(w)} = 0.1356$, S is the cross section area, h_0 is the hypothetical magnetic field controlled by the surrounding microenvironment of the material, and ρ_e is the resistivity [10]. The value of b of the HBN core is about one-half of the Fe-AM core. The values of ρ_e for the HBN core and Fe-AM core are ~0.8 and 1.3 μWm, respectively. Therefore, h_0 of the Fe-AM core can be estimated about 6.5 times larger than that of the HBN core. Since excess eddy current loss is a function of $f^{1.5}$, difference of core loss between the HBN core and the Fe-AM core is enhanced in the higher frequencies. Table II shows B_m at each frequency when the core loss becomes 12 W/kg. Here, 12 W/kg or ~100 kW/m^3 is the highest limit of acceptable heat. The HBN core can be operated by 15%–25% higher B_m than the Fe-AM core. In addition, because of the larger B_{2000} of the HBN core, we can expect at least 30% higher power from the HBN core than the Fe-AM core.

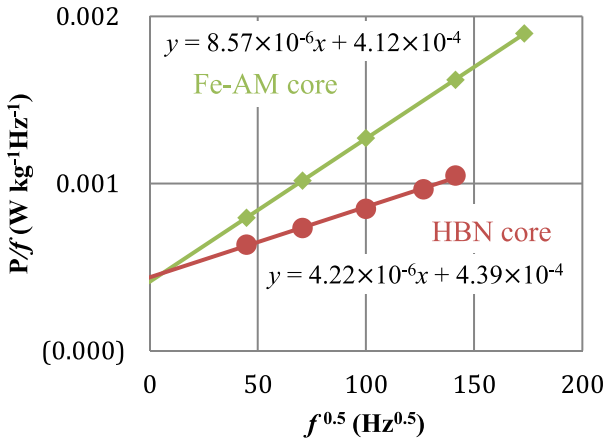

Fig. 5. P/f versus $f^{0.5}$ plot of block cores comprising HBN core and Fe-AM core.

TABLE II
B_m OF EACH FREQUENCY WHEN THE CORE LOSS BECOMES 12 W/kg

	High B nano B_m (mT)	SA1 B_m (mT)
10 kHz	233	200
20 kHz	150	120

Note that λ_s of the $Fe_{bal.}Cu_1Mo_{0.2}Si_4B_{14}$ nanocrystalline alloy is still high, so a large stress may cause an abrupt increase in the core loss. Fig. 6 shows the magnetic domain structure change from 0 to 80 A/m for a single sheet of annealed HBN cores with the curvature radius of 300 and 600 mm. These ribbons were restricted to be flat; hence compressing stress was applied on the surface. As seen in Fig. 6, the ribbon with the curvature radius of 600 mm shows faster magnetic saturation compared with the radius of curvature of 300 mm. During the molding process, the curvature of the ribbon is made to be flat, and larger stress is produced in the ribbon with the radius of curvature of 300 mm. The coefficient of

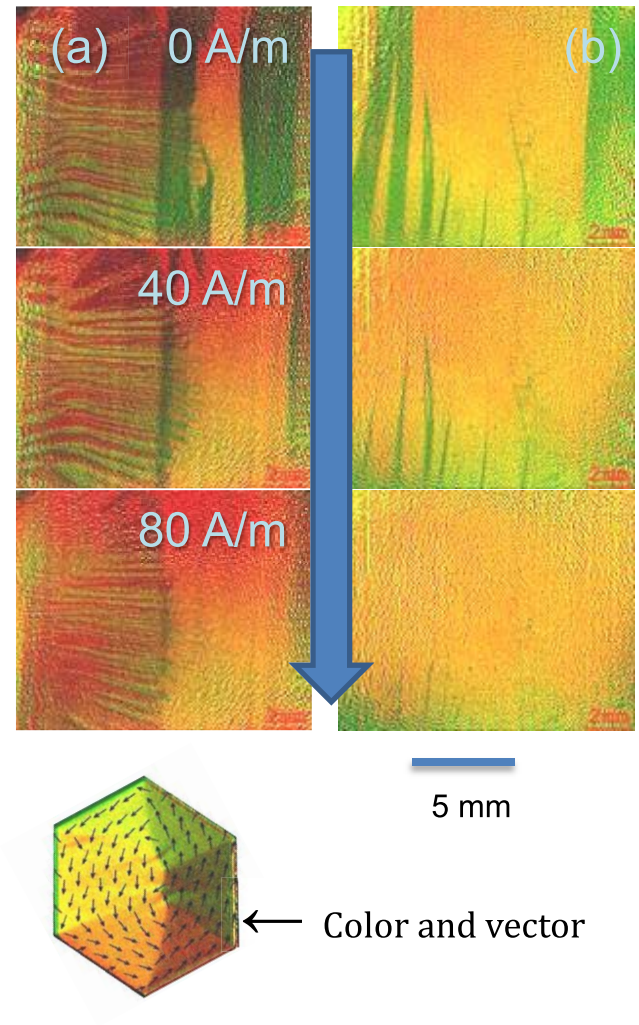

Fig. 6. Domain structure of annealed HBN core with a curvature radius of (a) 300 mm and (b) 600 mm.

excess eddy current b of a block core assembled with the ribbons with the curvature radius of 600 mm is 20% lower than that for the ribbon with the radius of curvature of 300 mm. According to our previous study, when a toroidal core is assembled, secondary annealing should be applied so that the residual stress is relieved [9]. In this paper, the ribbon was annealed to have a radius of curvature larger than 500 mm, and hence, secondary annealing was not necessary. Moreover, blocks have more size flexibility than toroidal cores. These findings can be of great benefit for the present block core in the application field of medium frequency power inductive components such as reactors in electrical vehicles, rail ways, and so on.

IV. Conclusion

The HBN core and their soft magnetic properties were tested in comparison to those of the Fe-AM core.

1) The HBN core shows magnetic flux density, B_{2000}, of 1.73 T at 2000 A/m, with 0.2 T increase as compared with the Fe-AM core.
2) The HBN core demonstrates a core loss of 8.5 W/kg at 200 mT and 10 kHz, which is two thirds of that of the Fe-AM core.
3) The core loss is found to arise from the excess eddy current at moderate frequencies. Since the coefficient of the excess eddy current of the HBN core is one half of that of the Fe-AM core, the contrast between their core losses would be enhanced at higher frequencies.

References

[1] G. Ortiz, M. Leibl, J. W. Kolar, and O. Apeldoorn, "Medium frequency transformers for solid-state-transformer applications—Design and experimental verification," in *Proc. IEEE 10th Int. Conf. Power Electron. Drive Syst.*, Apr. 2013, pp. 1285–1290.

[2] D. Rothmund, G. Ortiz, T. Guillod, and J. W. Kolar, "10kV SiC-based isolated DC–DC converter for medium voltage-connected solid-state transformers," in *Proc. IEEE Appl. Power Electron. Conf. Expo.*, Mar. 2015, pp. 1096–1103.

[3] ABB Review Special Report. *Shrinking the Core*. [Online]. Available: http://search-ext.abb.com/library/Download.aspx?DocumentID=9AKK105713A2321&LanguageCode=en&DocumentPartId=&Action=Launch

[4] D. Aggeler, J. Biela, and J. W. Kolar, "A compact, high voltage 25 kW, 50 kHz DC–DC converter based on SiC JFETs," in *Proc. 23rd Annu. IEEE Appl. Power Electron. Conf. Expo.*, Feb. 2008, pp. 801–807.

[5] M. A. Khan, G. Simin, S. G. Pytel, A. Monti, E. Santi, and J. L. Hudgins, "New developments in gallium nitride and the impact on power electronics," in *Proc. IEEE 36th Power Electron. Spec. Conf.*, Jun. 2005, pp. 15–26.

[6] (2015). *Super Core*. [Online]. Available: http://www.jfe-steel.co.jp/en

[7] T. Hiratani, M. Namikawa, and Y. Nishina, "Recent progress of high silicon electrical steel in JFE steel," JFE, Tokyo, Japan, Tech. Rep. 21, Mar. 2016.

[8] (2016). *Metglas Series Cut Core/FINEMET F3CC Series Cut Core*. [Online]. Available: https://www.hitachi-metals.co.jp/e

[9] M. Ohta and Y. Yoshizawa, "New high-B_s Fe-based nanocrystalline soft magnetic alloys," *Jpn. J. Appl. Phys.*, vol. 46, nos. 20–24. p. L477, 2007.

[10] M. Ohta and Y. Yoshizawa, "Magnetic properties of nanocrystalline $Fe_{82.65}Cu_{1.35}Si_xB_{16-x}$ alloys (x =0–7)," *Appl. Phys. Lett.*, vol. 91, no. 6, p. 062517, 2007.

[11] M. Ohta and Y. Yoshizawa, "Effect of heating rate on soft magnetic properties in nanocrystalline $Fe_{80.5}Cu_{1.5}Si_4B_{14}$ and $Fe_{82}Cu_1Nb_1Si_4B_{12}$ alloys," *Appl. Phys. Exp.*, vol. 2, no. 2, p. 023005, 2009.

[12] M. Ohta and Y. Yoshizawa, "High B_s nanocrystalline $Fe_{84-x-y}Cu_xNb_ySi_4B_{12}$ alloys (x =0.0–1.4, y =0.0–2.5)," *Magn. Magn. Mater.*, vol. 321, pp. 2220–2224, Jul. 2009.

[13] M. Ohta and R. Hasegawa, "Soft magnetic properties of magnetic cores assembled with a high B_s Fe-based nanocrystalline alloy," *IEEE Trans. Magn.*, vol. 53, no. 2, Feb. 2017, Art. no. 2000205.

[14] Y. Sakaki, "An approach estimating the number of domain walls and eddy current losses in grain-oriented 3% Si-Fe tape wound cores," *IEEE Trans. Magn.*, vol. MAG-16, no. 4, pp. 569–572, Jul. 1980.

[15] M. A. Willard, T. Francavilla, and V. G. Harris, "Core-loss analysis of an (Fe, Co, Ni)-based nanocrystalline soft magnetic alloy," *J. Appl. Phys.*, vol. 97, no. 10, p. 10F502, 2005.